

TDD frame design for interference handling in mobile IAB networks

Victor F. Monteiro¹, Fco. Rafael M. Lima¹, Darlan C. Moreira¹, Diego A. Sousa^{1,2},
Tarcisio F. Maciel¹, Behrooz Makki³, Ritesh Shreevastav³ and Hans Hannu³

Abstract—Integrated access and backhaul (IAB) is envisioned as a possible solution to address the need for network densification in situations where fiber connection is not viable. In Release 18, 3rd generation partnership project (3GPP) will take another step on extending IAB capabilities. With mobile IAB (mIAB), IAB nodes can be deployed within vehicles, e.g., buses. As in every new technology, performance assessment and evaluation of the impact of interference is of interest for industry and academia. In this paper, we present contributions on those topics. First, we evaluate the performance of mIAB compared to fiber-connected deployments. Moreover, we study the impact of interference on the performance of mIAB networks and propose a solution based on inserting silent slots on the time division duplex (TDD) frame pattern. According to our simulation results, mIAB is capable of improving performance of onboard user equipments (UEs) without harming too much the quality of service (QoS) of surrounding UEs. Furthermore, we show that the TDD frame pattern should be carefully designed to account for scenarios with different levels of interference.

Index Terms—IAB, mobile IAB, wireless backhaul, 5G standardization, 6G, mobility, moving cell, relay.

I. INTRODUCTION

Network densification has been an effective solution to the challenges faced by mobile communication systems such as the increased number of connected terminals, new multimedia services and high required data rates [1]. However, the increased number of base stations per area also demands an improved backhaul infrastructure. Fiber is the default choice, if available, to provide backhaul connection from base stations to the core network. Nevertheless, there are two main drawbacks when deploying fiber for backhaul connection [2], [3]: i) depending on the region, the cost to deploy fiber for backhaul, e.g., trenching and installation, can be high especially when dark fiber is not available; ii) in general, the deployment of fiber for backhaul takes time and can even be impossible in, e.g., historical places where trenching is not an option.

Wireless backhaul is a good complement to fiber. In fact, wireless backhaul technology has been deployed in mobile networks for a long time mainly using proprietary solutions and dedicated spectrum [4]. In Release 10, 3GPP standardized wireless backhaul for long term evolution (LTE), the so called LTE relaying [5]. However, the commercial interest was not as large as expected, due to, e.g., the

This work was supported by Ericsson Research, Sweden, and Ericsson Innovation Center, Brazil, under UFC.49 Technical Cooperation Contract Ericsson/UFC. The work of Fco. Rafael M. Lima was supported by FUNCAP (edital BPI) under Grant BP4-0172-00245.01.00/20. The work of Tarcisio F. Maciel was supported by CNPq under Grant 312471/2021-1.

¹ Wireless Telecommunications Research Group (GTEL), Federal University of Ceará (UFC), Fortaleza, Ceará, Brazil; ² Federal Institute of Education, Science, and Technology of Ceará (IFCE), Paracuru, Brazil; ³ Ericsson Research, Sweden.

small available spectrum resources and lack of use-case of interest at that time. Motivated by the large bandwidths available in millimeter wave (mmWave) spectrum employed in fifth generation (5G) networks and advanced multiple input multiple output (MIMO) techniques, 3GPP began the first studies on wireless backhaul for new radio (NR) in 2017 under the name of IAB [6].

The first set of specifications of IAB was frozen on July 2020 in Release 16 [7]. Optimization of some functionalities and increased efficiency are the focus of Release 17 for IAB that should have its stage 3 protocol frozen on early 2022. In December 2021, 3GPP presented the package approval for Release 18 setting the cornerstone for 5G advanced. Under the name of mIAB, a work item will specify protocols and procedures needed to provide wireless backhaul under IAB to moving nodes [8].

In this paper, we show that mIAB networks is a possible solution to improve QoS for UEs onboard of busses, compared to classical solutions such as the deployment of fiber-based macro/pico cells. Furthermore, we study an mIAB network over different interference conditions and transmission configurations. More specifically, we assume two distinct system layouts: one limited and another non-limited by interference. Furthermore, we assume different TDD frame patterns where backhaul and access transmissions can or cannot take place simultaneously. Our objective is to evaluate *when and over which mIAB transmission configurations* the interference level becomes unbearable.

II. BACKGROUND

A. Integrated access and backhaul

As illustrated in Fig. 1, an IAB network has two main components: IAB donor and IAB node. The IAB donor provides a wireless backhaul to IAB nodes allowing these to provide access to their served UEs.

Concerning the IAB donor, it is split in centralized unit (CU) and distributed units (DUs). This split is transparent to the served UEs and these units can be either collocated or non-collocated. In the IAB donor, the DU terminates lower protocol layers, e.g., physical (PHY), medium access control (MAC), and radio link control (RLC), while the CU terminates upper protocol layers, e.g., packet data convergence protocol (PDCP) and radio resource control (RRC). The motivation for the Rel-16 chosen architecture was centralization (not having a CU in every IAB-node), equivalent to lean IAB nodes.

Regarding the IAB nodes, they support gNodeB (gNB) DU and mobile termination (MT) functions, as illustrated in Fig. 1. On the one hand, the IAB-MT terminates the radio interface layers of its backhaul towards an upstream IAB donor or

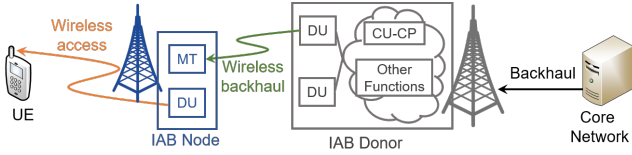


Fig. 1. Example of IAB NR architecture.

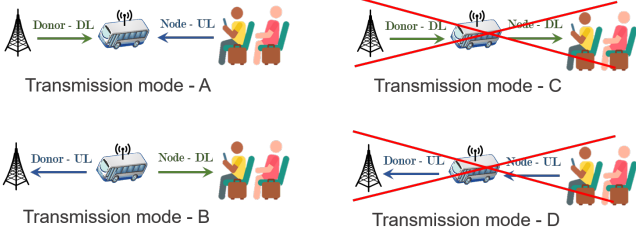


Fig. 2. List of possible simultaneous operation modes.

parent IAB. On the other hand, the IAB-DU terminates the NR interface to UEs and/or child IAB nodes. For compatibility purposes with legacy networks, the IAB-MT acts not different from a UE from the point-of-view of its parent IAB. From a UE point of view, the IAB-DU looks like as the DU of a regular gNB.

As already mentioned, in 3GPP Release 18, different radio access network (RAN) working groups will work towards enhancing functionalities of IAB focusing on mIAB to provide 5G services to onboard UEs. One of the main use-cases of mIAB cells is to serve UEs onboard of, e.g., busses. Some advantages of mIAB are to improve connectivity to the network by reducing/eliminating the vehicle penetration loss (especially at high frequency) and to avoid signalling storms from simultaneous handover (HO) messages.

B. Interference in mIAB Scenario

A challenge that appears in scenarios with mIAB is the interference management. Two major types of interference in these scenarios are the self-interference and the dynamic interference between mobile and legacy deployed stationary cells that may occur when they share frequency spectrum. These two types of interference are explained in the following.

Figure 2 presents 4 possible simultaneous transmission modes in which an mIAB can operate. In modes A and B, the DU and MT parts of an mIAB node perform the same actions (either receive or transmit data), while in modes C and D they perform opposite actions. Modes C and D are often referred to as IAB full duplex (FD) modes, where the MT-part of the mIAB node receives data in the backhaul while its DU-part transmits data to access UE, or vice versa. In IAB FD modes, the part which is transmitting may cause strong interference to the part that is receiving, which is the so called self-interference.

Self-interference can only be mitigated in very specific implementations and scenarios, e.g., where both DU and MT parts of the mIAB node are very isolated from each other or complex signal processing strategies in analog and digital domains are employed. Thus, in order to avoid the problem of self-interference, the network usually allows an mIAB node to only operate in transmission modes A and B, resulting

TABLE I
TDD SCHEME AVOIDING SELF-INTERFERENCE.

Slot	1	2	DL usage	UL usage	Total usage
IAB donor access	DL	UL	50%	50%	100%
mIAB node backhaul	DL	UL	50%	50%	100%
mIAB node access	UL	DL	50%	50%	100%

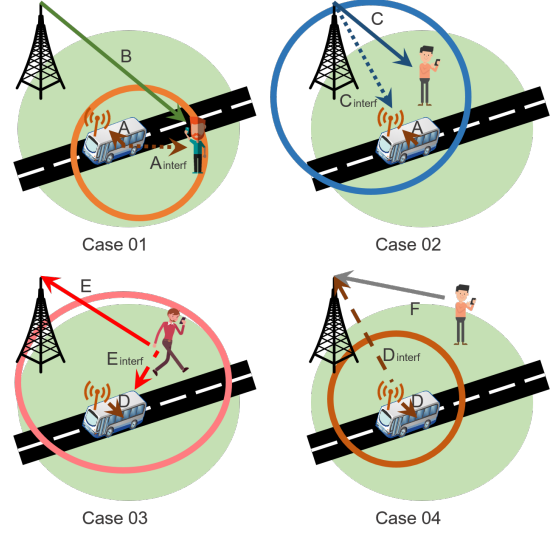


Fig. 3. Examples of interference in mIAB scenario.

in the TDD scheme showed in Table I (for an IAB network operating with a maximum of two hops, i.e., where an mIAB node cannot be served by another mIAB node).

The TDD scheme in Table I may cause dynamic interference between mIAB cells and crossed fixed cells. Figure 3 illustrates the two cases (Cases 01 and 02) of interference that occur when the IAB donor is in downlink (DL) and the mIAB node in uplink (UL), and the two cases (Cases 03 and 04) when the IAB donor is in UL and the mIAB node in DL.

More specifically, in Case 01, a pedestrian receiving data in the DL (link B) from an IAB donor may suffer interference (link A_{interf}) from an in-vehicle passenger transmitting in the UL (link A) to an mIAB node deployed inside a bus. In Case 02, the DU part of an mIAB node receiving data in the UL (link A) from a passenger may suffer interference (link C_{interf}) from the IAB donor when it transmits in the DL (link C) to a pedestrian. In Case 03, a passenger receiving data from an mIAB node in the DL (link D) may suffer interference (link E_{interf}) from a pedestrian transmitting in the UL to its serving IAB donor (link E). In Case 04, an IAB donor receiving data in the UL (link F) from a pedestrian may suffer interference (link D_{interf}) from the DU part of an mIAB node transmitting in the DL (link D).

III. PROBLEMS WITH EXISTING SOLUTIONS AND PERSPECTIVES

The dynamic interference between moving cells and fixed cells can limit the network performance. Some solutions can be envisaged to tackle this problem.

A first option is to assume that the mIAB network operates with two distinct frequency bands: one to serve onboard UEs and another to serve surrounding UEs. For example, short

TABLE II
TDD SCHEME WITH SILENT SLOTS.

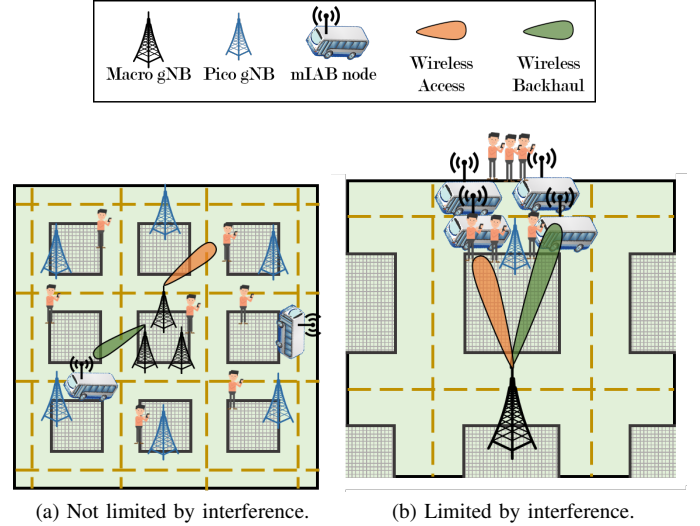
Slot	1	2	3	4	5	6	7	8	9	10	DL usage	UL usage	Total usage
IAB donor access	DL	UL	-	DL	-	UL	DL	-	UL	DL	40%	30%	70%
IAB node backhaul	DL	-	UL	DL	UL	-	-	UL	-	DL	30%	30%	60%
IAB node access	-	UL	DL	-	DL	UL	DL	DL	UL	-	40%	30%	70%

range mmWave spectrum could be assigned to onboard UEs while sub-6 GHz could be used to serve surrounding UEs. The main disadvantage of this solution is that the load in mIAB can be very dynamic and, in some cases, the bandwidth available in mmWave spectrum may remain unused, e.g., when the load offered by onboard UEs is low.

An alternative to this inflexible frequency partitioning is to employ dynamic time-frequency resource allocation where the whole bandwidth would be available to the time-frequency schedulers. In this case, IAB donor and mIAB nodes could coordinate their transmissions in order to dynamically control the interference level in the system. The schedulers can take their decisions based, for example, on interference information and on the system load. Although we expect that this solution can substantially improve the system performance, this would be obtained at the cost of increased complexity and signalling load. More specifically, up-to-date system information such as interference and load measurements should be available at nodes where decision would be taken. Moreover, those measurements should be frequently collected, since they can vary a lot in such a dynamic network.

Thus, in this paper we evaluate the potential of a different alternative to deal with interference in mIAB network. In fact, in order to control the interference between the links as shown in Fig. 3, a TDD frame different from the one shown in Table I can be designed. More specifically, silent slots can be inserted in the TDD frame structure as, e.g., shown in Table II. Note that in this TDD frame structure, in some slots either the link involving IAB donor access, mIAB node access or backhaul is disabled, i.e., no transmission/reception of data is allowed. These slots are called here in as *slots of silence*. Therefore, some of the interference cases shown in Fig. 3 can be avoided. For example, in Slot 1, as mIAB node access is disabled, the interference Case 01 in Fig. 3 is not an issue anymore, as the pedestrian UE would not receive interference from UL transmissions from UEs connected to the mIAB. In Slot 3, for example, as IAB donor access is disabled, interference Case 03 does not hold since onboard UEs connected to the mIAB would not experience interference from pedestrian UEs (connected in UL to the IAB donor).

There is a clear trade-off when employing silent slots for interference handling. On the one hand, a lower interference is experienced in the whole system as previously explained. This leads to an improved signal level which can be translated in the use of higher-order modulation and coding schemes (MCSs). On the other hand, as some of the links are blocked depending on the slot, the overall TDD frame efficiency decreases. For example, switching from the TDD frame shown in Table I to the one in Table II, the active period of the IAB donor access drops from 100% to 70%. In this case, there are less opportunities to transmit which can lead to reduced



(a) Not limited by interference.

(b) Limited by interference.

Fig. 4. Scenarios of interest.

throughput. Thus, in Section IV we will evaluate the impact of the use of TDD frame patterns with and without slots of silence in scenarios with different levels of interference.

IV. PERFORMANCE EVALUATION

This section presents a performance comparison between a scenario with mIAB and two benchmark scenarios, i.e., a scenario with only macro gNBs, called here as *only macros* scenario and other with macro and pico gNBs fiber-connected to the core network (CN), called here as *macros-picos* scenario. The details concerning the considered simulation modelling are presented in Section IV-A and the results are discussed in Section IV-B.

A. Simulation Assumptions

In order to perform the simulations, two system layouts were considered. They were based on the Madrid grid [10]. The first layout, Fig. 4a, was not limited by interference, while the second one, Fig. 4b, was limited by interference.

In the layout not limited by interference, Fig. 4a, there were nine $120\text{ m} \times 120\text{ m}$ blocks. They were surrounded by 3 m wide sidewalks and separated of each other by 14 m wide streets with four lanes, two in each direction. In the central block there were 3 not co-located macro gNBs. Pedestrians and buses were initially randomly placed in the sidewalks and in the streets, respectively. In the intersections, they had a probability of 60 % to continue straight ahead, 20 % to turn left and 20 % to turn right. The pedestrians walked in the sidewalks and were allowed to cross the roads only in the intersections. Passengers were randomly located inside the buses at any available seat. During the simulation, their position relative to their bus did not change. In the macros-picos scenario, in addition to the three macro gNBs, there were six pico gNBs

TABLE III
TDD SCHEME ADOPTED IN ONLY MACROS AND MACROS-PICOS SCENARIOS.

Slot	1	2	3	4	5	6	7	8	9	10	DL usage	UL usage	Total usage
Macro gNBs	DL	S (DL)	UL	UL	UL	DL	S (DL)	UL	UL	DL	50%	50%	100%

TABLE IV
ENTITIES CHARACTERISTICS.

Parameter	IAB Donor	mIAB node - DU	mIAB node - MT	Pedestrian	Passenger
Height	25 m	2.5 m	3.5 m	1.5 m	1.8 m
Transmit power	35 dBm	24 dBm	24 dBm	24 dBm	24 dBm
Antenna tilt	12°	4°	0°	0°	0°
Antenna array	URA 8 × 8	URA 8 × 8	ULA 64	Single antenna	Single antenna
Antenna element pattern	3GPP 3D [9]	3GPP 3D [9]	Omni	Omni	Omni
Max. antenna element gain	8 dBi	8 dBi	0 dBi	0 dBi	0 dBi
Speed (not limited by interference)	0 km/h	40 km/h	40 km/h	3 km/h	40 km/h
Speed (limited by interference)	0 km/h	20 km/h	20 km/h	3 km/h	20 km/h

TABLE V
SIMULATION PARAMETERS.

Parameter	Value
Carrier frequency	28 GHz
System bandwidth	50 MHz
Subcarrier spacing	60 kHz
Number of subcarriers per RB	12
Number of RBs	66
Slot duration	0.25 ms
OFDM symbols per slot	14
Channel generation procedure	As described in [9, Fig.7.6.4-1]
Path loss	Eqs. in [9, Table 7.4.1-1]
Fast fading	As described in [9, Sec.7.5] and [9, Table7.5-6]
AWGN power per subcarrier	-174 dBm
Noise figure	9 dB
Number of buses	6
Passengers + pedestrians	72
Percentage of passengers	50%
Number of passengers per bus	6
CBR packet size	3072 bits
CBR packet inter-arrival time	4 slots

deployed as indicated in Fig. 4a (at the vertices of a hexagon). In the mIAB scenario, mIAB nodes were deployed at the buses. The DU and MT were placed at the back of the buses; however, the DU was inside and the MT was outside at the roof. An mIAB node could not connect to another mIAB node, but only be served by an IAB donor, i.e., a gNB.

Concerning the layout limited by interference, i.e., Fig. 4b, it had two main differences compared to the layout not limited by interference: i) pedestrians, buses and passengers from the previous layout were concentrated in just one block, and; ii) there was just one macro gNB instead of three as in the previous layout.

Regarding resource scheduling, the TDD scheme presented in Table III and standardized by 3GPP in [11] was considered in the only macros and macros-picos scenarios. For the IAB, in each scenario, two TDD schemes were considered: one without and other with slots of silence, as presented in Table I and Table II, respectively.

The 5G-SToRM channel model [12] was used to model the channel of the links. It is an implementation of [9]. It is spatially- and time-consistent and considers a distance-dependent path-loss, a lognormal shadowing

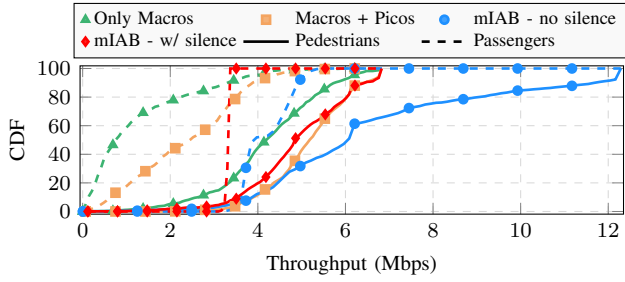
component and small-scale fading. Moreover, all links with the IABdonor, i.e., IABdonor to pedestrian, mIAB-MT, mIAB-DU and passenger, were modelled as urban macro (UMa). All links involving the mIAB-MT, except the link IAB donor - mIAB-MT, were modelled as urban micro (UMi), as well as the links pedestrian to mIAB-DU and passenger. The link DU-passenger was modelled as an indoor hotspot. The bus body had a penetration loss of 20 dB [13]. Thus, the links between one entity inside the bus and another outside, such as {IAB donor - mIAB-DU}, {mIAB-DU - pedestrian}, { mIAB-MT - passenger}, and {pedestrian - passenger}, suffered this penetration loss. Furthermore, the link between a DU of a bus and a passenger of another bus suffered twice this penetration loss. Besides, all links that crossed the bus body were considered non-line of sight (NLOS). The other links could be either in line of sight (LOS) or NLOS with a transitional state between them as described in [9].

UEs and mIAB nodes measured the reference signal received power (RSRP) of candidate serving cells as defined in [14]. The topology adaptation, i.e., selection of IAB donor, was based on the highest measured RSRP. Concerning the link adaptation, it was adopted the channel quality indicator (CQI)/MCS mapping curves standardized in [15] with a target block error rate (BLER) of 10%. We also considered an outer loop strategy to avoid the increase of the BLER. According to this strategy, when a transmission error occurred, the estimated signal to interference-plus-noise ratio (SINR) used for the CQI/MCS mapping in the link adaptation was subtracted by a back-off value of 1 dB and, when a transmission occurred without error, the estimated SINR had its value added by 0.1 dB. Tables IV and V present other relevant simulation parameters.

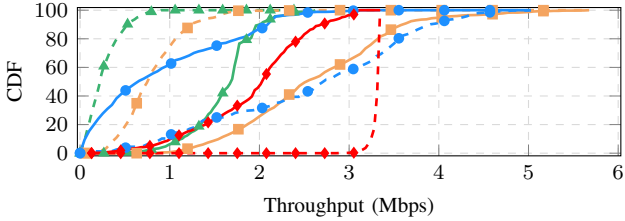
B. Simulation Results

Let us analyze the impact of introducing mIAB with and without slots of silence on the DL throughput of passengers and pedestrians presented in Fig. 5. More specifically, Fig. 5a and Fig. 5b refer to the scenarios not limited and limited by interference, respectively.

First, notice in Fig. 5a that, in the scenario not limited by interference, deploying mIAB nodes with and without slots of silence outstandingly improved the passengers' DL throughput



(a) Layout not limited by interference.



(b) Layout limited by interference.

Fig. 5. The CDF of DL throughput for different interference scenarios.

compared to the cases of only macros and macros-picos. While in the only macros and macros-picos only 11% and 31%, respectively, of the passengers had DL throughput higher than 3.2 Mbits/s, with the mIAB almost all the passengers had DL throughput higher than 3.2 Mbits/s. Moreover, since in this scenario the interference was not a problem, having slots of silence was a waste of resources. Hence, the mIAB without slots of silence, i.e., always available for transmission, outperformed the case of mIAB with slots of silence.

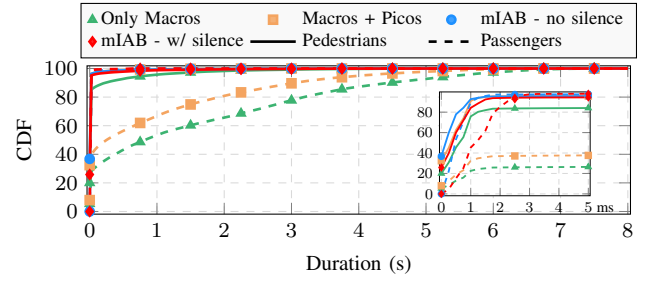
In the scenario limited by interference, Fig. 5b, passengers were also benefited by the deployment of mIAB nodes with or without slots of silence. However, in this scenario, mIAB without slots of silence harmed more the access links of pedestrians than those of passengers. This occurred because the passengers were close to the serving antennas, reducing the impact of interference, while the pedestrians were further to their serving gNB than to the interference source, i.e., passengers transmitting in the UL according to Table II.

Regarding the DL latency, Fig. 6 presents the CDF of DL latency for pedestrians and passengers in all considered cases. Notice that, in the scenario not limited by interference, Fig. 6a, on the one hand mIAB presented DL latency lower than 5 ms for at least 90% of both pedestrians and passengers. On the other hand, the only macros and macros-picos cases presented DL latency greater than 0.5 s for the majority of the passengers, with some of them facing a delay higher than 5 s. This fact highlights that having only macros and/or picos is not enough to provide a good connection to onboard passengers.

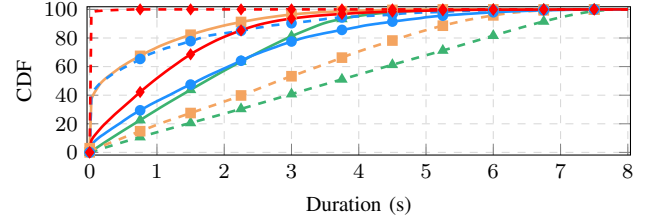
Figure 7 presents the average of the total amount of bits transmitted in the DL by each solution. Since there were 36 passengers and 36 pedestrians, the amount of generated bits in the DL to passengers and pedestrians was equal to:

$$36 \text{ UEs} \left(\frac{1 \text{ packet}}{4 \text{ slots}} \right) \left(\frac{1 \text{ slot}}{0.25 \text{ ms}} \right) \left(\frac{8,000 \text{ ms}}{\text{simulation}} \right) \left(\frac{3,072 \text{ bits}}{1 \text{ UE} \times 1 \text{ packet}} \right) = 884.7 \text{ Mbits/simulation.} \quad (1)$$

First, notice that, even though in the scenario not limited

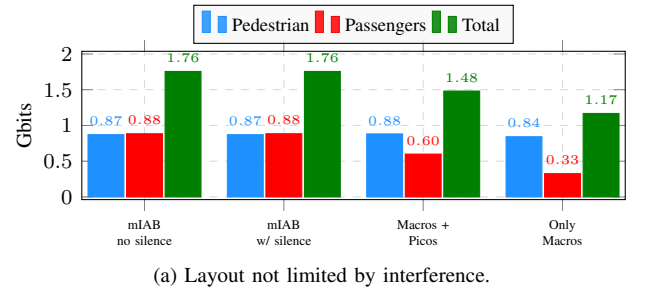


(a) Layout not limited by interference.

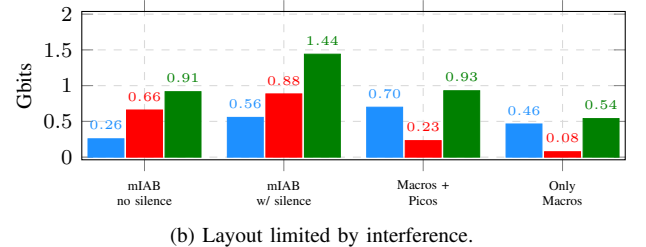


(b) Layout limited by interference.

Fig. 6. DL latency.



(a) Layout not limited by interference.

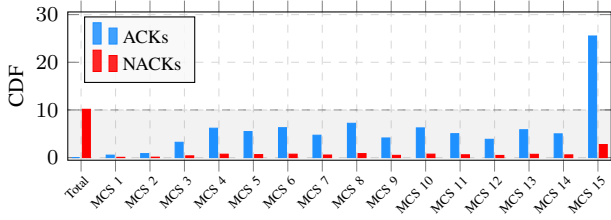


(b) Layout limited by interference.

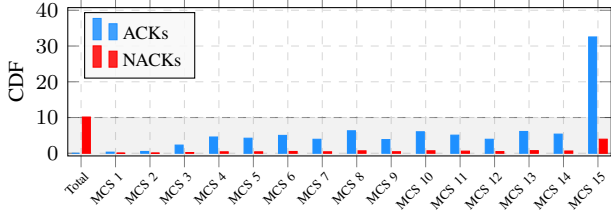
Fig. 7. Total transmitted bits.

by interference the mIAB with slots of silence presented lower DL throughput compared to the mIAB without slots of silence, as shown in Fig. 5a, both solutions were able to deliver almost all the generated data to pedestrians and passengers, as presented in Fig. 7a. Moreover, comparing how their performances changed when switching from a scenario not limited by interference, Fig. 7a, to a scenario limited by interference, Fig. 7b, we can see that: i) the mIAB without slots of silence was severely impacted by the interference, and; ii) the pedestrians were more affected than the passengers. This occurred because the passengers were close to the transmitting antennas, reducing the impact of interference, while the pedestrians were closer to the interference source than to the serving gNB. Important to remark that in the layout limited by interference, the passengers received less than 10% and 26% of the generated data in the only macros and macro-picos scenarios, respectively.

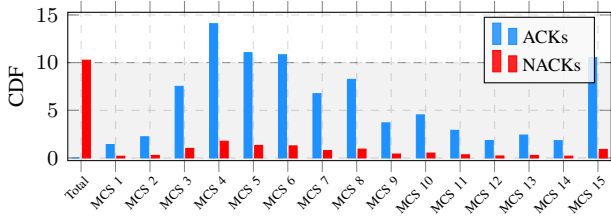
Until now, the analyses focused on the access links. Let us



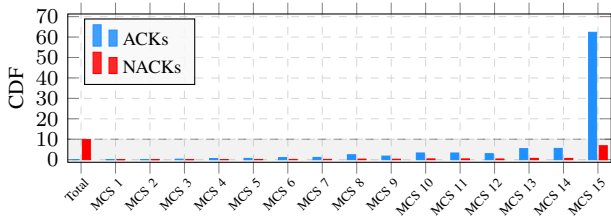
(a) Layout not limited by interference and TDD scheme without slot of silence.



(b) Layout not limited by interference and TDD scheme with slot of silence.



(c) Layout limited by interference and TDD scheme without slot of silence.



(d) Layout limited by interference and TDD scheme with slot of silence.

Fig. 8. Backhaul MCS usage.

now analyze, in Fig. 8, the histogram of MCS usage in the backhaul link of the mIAB nodes. Figures 8a and 8b concern the cases without and with slots of silence, respectively, in the scenario not limited by interference. Comparing these two figures, we can see that in this scenario both solutions were able to transmit data in the backhaul using the highest MCS. As expected, in the layout limited by interference, mIAB without slots of silence, Fig. 8c, had its backhaul affected by the interference impacting the used MCSs.

Comparing Figs. 8b and 8d, notice that for the mIAB solution with slots of silence, when we moved from the layout not limited by interference to the scenario limited by interference, the quality of the backhaul improved. This is due to the fact that when the backhaul was in DL, i.e., the mIAB-MT was receiving, the main interference came from the onboard UEs transmitting in the UL to the mIAB-DU. The distance between the mIAB-MT and the onboard UEs (source of interference) was approximately constant, thus

changing the scenario did not considerably change the level of interference in the backhaul. However, in the scenario limited by interference, the mIAB nodes were closer to the serving IAB donor, which increased the strength of the received signal.

V. CONCLUSIONS

We concluded that mIAB has the potential to improve the throughput and latency of UEs onboard of busses, which poorly performed in the considered benchmark scenarios, i.e., with only macro and/or pico gNBs. More specifically, mIAB with a TDD scheme with slots of silence outperformed benchmark solutions in scenarios with different levels of interference. Furthermore, in a considered scenario, which was not limited by interference, a TDD scheme without slots of silence performed even better. Thus, since a TDD scheme with slots of silence performed well in both scenarios, it could be adopted as a default solution. Moreover, depending on the data traffic, geographical conditions, etc. it may be useful to adapt the TDD scheme.

REFERENCES

- [1] V. Jungnickel, K. Manolakis, W. Zirwas, B. Panzner, V. Braun, M. Lossow, M. Sternad, R. Apelfröjd, and T. Svensson, "The role of small cells, coordinated multipoint, and massive mimo in 5G," *IEEE Commun. Mag.*, vol. 52, no. 5, pp. 44–51, May 2014. DOI: 10.1109/MCOM.2014.6815892.
- [2] C. Madapatha, B. Makki, C. Fang, O. Teyeb, E. Dahlman, M.-S. Alouini, and T. Svensson, "On integrated access and backhaul networks: Current status and potentials," *IEEE Open J. Commu. Soc.*, vol. 1, pp. 1374–1389, Sep. 2020. DOI: 10.1109/OJCOMS.2020.3022529.
- [3] C. Madapatha, B. Makki, A. Muhammad, E. Dahlman, M.-S. Alouini, and T. Svensson, "On topology optimization and routing in integrated access and backhaul networks: A genetic algorithm-based approach," *IEEE Open J. Commu. Soc.*, vol. 2, pp. 2273–2291, Sep. 2021. DOI: 10.1109/OJCOMS.2021.3114669.
- [4] J. Edstam, A. Olsson, J. Flodin, M. Öhberg, A. Henriksson, J. Hansryd, and J. Ahlberg, "Ericsson microwave outlook," Ericsson, Stockholm, Sweden, Technical Report, Dec. 2018, pp. 2–16.
- [5] 3GPP, "Overview of 3GPP Release 10," 3rd Generation Partnership Project (3GPP), TR, Jul. 2014.
- [6] —, "NR; study on integrated access and backhaul (release 16)," 3rd Generation Partnership Project (3GPP), TR 38.874, Dec. 2018, v.16.0.0.
- [7] —, "NR; NR and NG-RAN Overall description; Stage 2," 3rd Generation Partnership Project (3GPP), TS 38.300, Jul. 2020, v.16.2.0.
- [8] —, "Summary for RAN Rel-18 Package," 3rd Generation Partnership Project (3GPP), RP 213469, Dec. 2021, TSG-RAN meeting no. 94.
- [9] —, "Study on channel model for frequencies from 0.5 to 100 GHz," 3rd Generation Partnership Project (3GPP), TR 38.901, Sep. 2017, v.14.2.0.
- [10] P. Agyapong *et al.*, "Simulation guidelines," METIS, Deliverable 6.1, Oct. 2013.
- [11] 3GPP, "Evolved universal terrestrial radio access (E-UTRA); physical channels and modulation," 3rd Generation Partnership Project (3GPP), TS 36.211, Jun. 2021, v.16.6.0.
- [12] A. M. Pessoa, I. M. Guerreiro, C. F. M. e Silva, T. F. Maciel, D. A. Sousa, D. C. Moreira, and F. R. P. Cavalcanti, "A stochastic channel model with dual mobility for 5G massive networks," *IEEE Access*, vol. 7, pp. 149 971–149 987, Oct. 2019, ISSN: 2169-3536. DOI: 10.1109/ACCESS.2019.2947407.
- [13] A. Mastro Simone and D. Panno, "Moving network based on mmWave technology: A promising solution for 5G vehicular users," *Wireless Netw.*, vol. 24, no. 7, pp. 2409–2426, Mar. 2017. DOI: 10.1007/s11276-017-1479-0.
- [14] 3GPP, "NR; physical layer measurements," 3rd Generation Partnership Project (3GPP), TS 38.215, version v.15.3.0, Sep. 2018.
- [15] —, "NR; physical layer procedures for data," 3rd Generation Partnership Project (3GPP), TS 38.214, Dec. 2017, v.15.0.0.